Hindawi
Journal of Nanomaterials
Volume 2022, Article ID 1033216, 9 pages
https://doi.org/10.1155/2022/1033216

Research Article

Analysis of Spectroscopic, Morphological Characterization and Interaction of Dye Molecules for the Surface Modification of TiB_2 Nanoparticles

S. Mayakannan,[1] R. Rathinam,[2] Rajasekaran Saminathan,[3] R. Deepalakshmi,[4] Mahesh Gopal,[5] J. Justin Maria Hillary,[6] S. Nanthakumar,[7] V. Y. Ganvir,[8] and Pallavi Singh[9]

[1]*Department of Mechanical Engineering, Vidyaa Vikas College of Engineering and Technology, Tiruchengode, Namakkal, Tamilnadu, India*
[2]*Department of Chemistry, Sri Eshwar College of Engineering, Coimbatore, 641202 Tamilnadu, India*
[3]*Mechanical Engineering, College of Engineering, Jazan University, Jazan city, Jazan, Saudi Arabia*
[4]*Computer Applications, Department of Inter-Disciplinary Studies, The Tamil Nadu Dr. Ambedkar Law University, Chennai, Tamilnadu, India*
[5]*Department of Mechanical Engineering, Wollega University, P.O. Box. 395 Nekemte, Ethiopia*
[6]*Department of Mechatronics Engineering, Sri Krishna College of Engineering and Technology, Coimbatore, Tamilnadu, India*
[7]*Department of Mechanical Engineering, PSG Institute of Technology and Applied Research Neelambur, Coimbatore, 641062 Tamilnadu, India*
[8]*Department of Applied Physics, Yeshwantrao Chavan College of Engineering, Nagpur, India*
[9]*Department of Biotechnology, Graphic Era Deemed to be University, Dehradun, Uttarakhand, India*

Correspondence should be addressed to Mahesh Gopal; doctorgmahesh@gmail.com

Received 4 September 2022; Accepted 30 September 2022; Published 15 October 2022

Academic Editor: Ridwan Yahaya

Nanoparticles of titanium diboride (TiB_2) coated with a conductive polymer and subjected to an oxidizing agent was carried out in this research. TiB_2 nanoparticles coated with polypyrrole (PPy) were studied using XRD and TEM techniques. Nitrogen adsorption and desorption properties of nanoparticles are covered with modified polypyrrole to understand better the surface zone, structural features, and pore geometries of the nanoparticles. The water-based hazardous anionic Congo red (CR) dye was removed using polypyrrole-coated titanium diboride (PPy@TiB_2) nanoparticles. Numerous cutting-edge experimental techniques, including FTIR, FE-SEM, EDXS, and element mapping analysis, were used to confirm the CR color's adhesion to the PPy@TiB_2 nanoadsorbent study. While conducting batch experiments, coated TiB_2 nanoadsorbents with polypyrrole enhanced the adsorption behaviour. One of the factors evaluated in the adsorption tests was pH; another was contact time, and a third was dose. At pH = 4, 98.75% of Congo red dye was detached using 60 mg of PPy-coated TiB_2 nanoadsorbent. Several sorption-desorption cycles were performed on this nanoadsorbent to determine its reusability. An excellent adsorption capacity for water treatment is reported in PPy-coated TiB2 nanoadsorbent.

1. Introduction

Every continent has a textile industry, and this sector contributes significantly to global economic growth [1]. Due to the coloring, printing, and washing processes carried without the appropriate pretreatment measures, textile wastewater is increasingly dyed. There are various concentrations of colored components in textile wastewater, which contribute

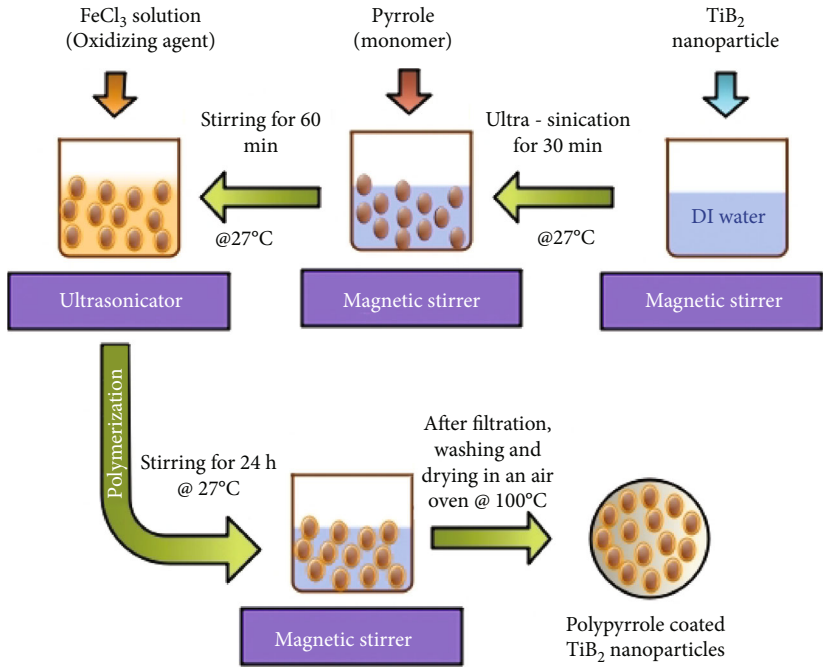

Figure 1: Diagram for the production of PPy@TiB_2.

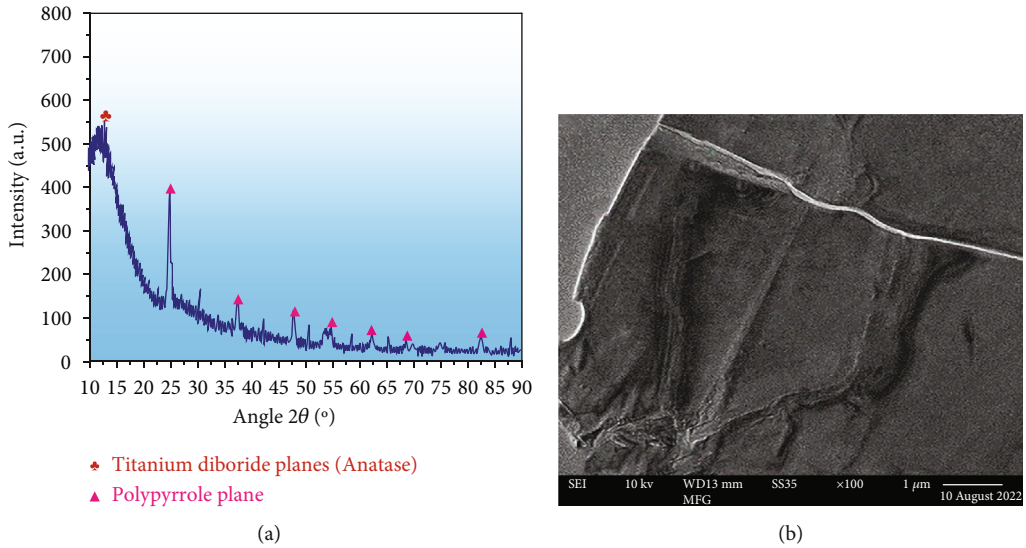

(a) (b)

Figure 2: (a) XRD and (b)TEM analysis of PPy@TiB_2.

to its pollution [2]. Therefore, textile effluent is clean since it has a high concentration of pigment molecules. Due to CR's ability to convert to benzidine, the anionic synthetic diazo dye is carcinogenic. Because of its aromatic structure, CR dye is both physiochemically and thermally stable [3]. CR's color changes depending on the pH, turning red at a pH of less than 5. Toxic to humans and animals, industrial effluent contains significant levels of COD and BOD, suspended particles and colloids, salts, and some other hard materials [4]. To deal with textile wastewater treatment issues, energy, water, and chemicals are required. There are numerous advantages to adsorption over other water treatment methods that are investigated as a viable option [5].

Various adsorbent forms are tried, including polar and nonpolar adsorbents. High surface-area adsorbent materials have effectively extracted different dye compounds from textile effluent. Various essential uses for nanomaterials have also been demonstrated [6–8]. Nanoparticles of titanium diboride (TiB_2) were employed in multiple material science applications: high-performance solar cells and photocatalytic devices using TiB_2-based nanotubes or nanoflowers, TiB_2 nanoparticles, and a PVDF membrane covered with a TiB_2 layer amplified for photocatalytic wastewater purification [9–11]. A polymer matrix alters the material's properties, such as combining polypropylene, polypyrrole, polyamide, or polylactic acid. Environmental scientists have

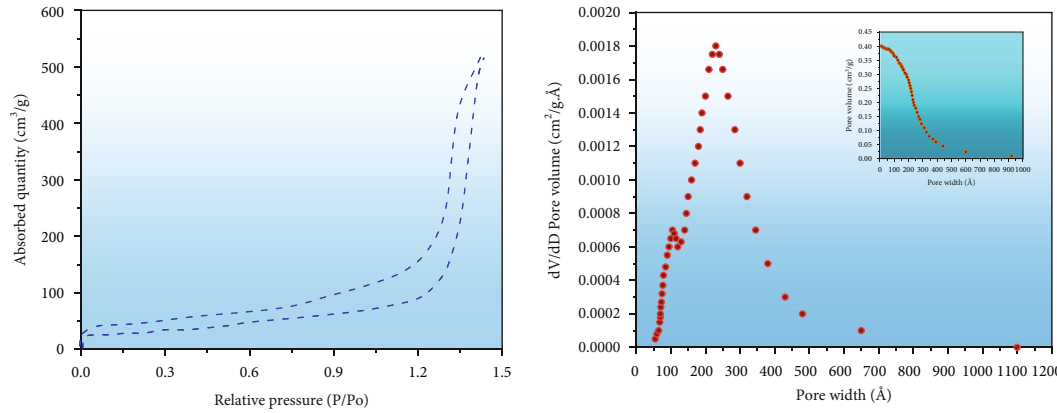

(a) (b)

Figure 3: (a) Isotherm of N-adsorbed and desorbed of PPy@TiB_2 and (b) grain size dispersal plot and comparison of pore width and volume plot.

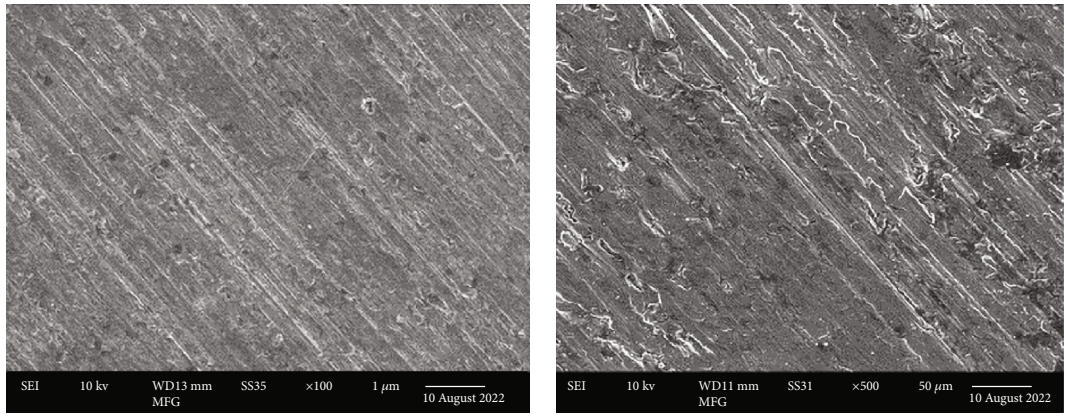

(a) (b)

Figure 4: FESEM images of various magnifications of (a) PPy@TiB_2 and (b) CR-adsorbed PPy@TiB_2.

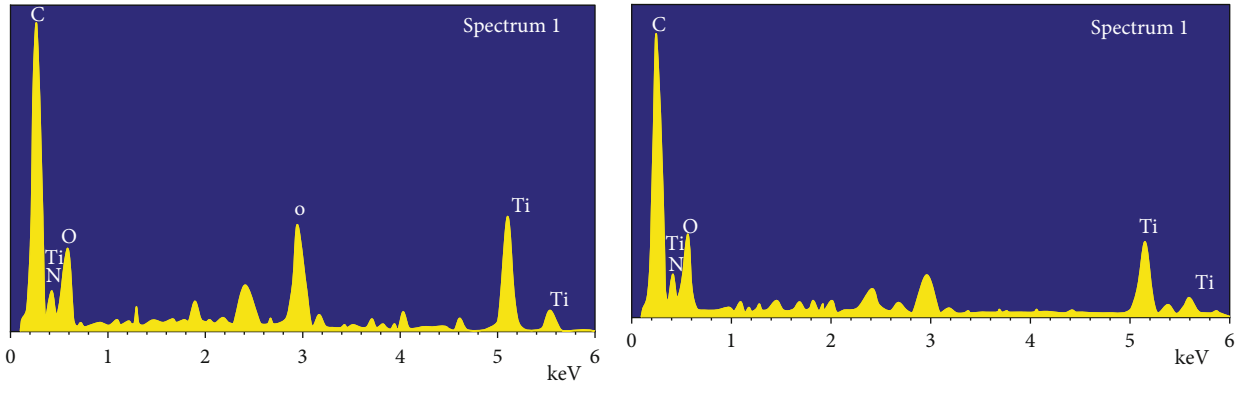

(a) (b)

Figure 5: Energy dispersive X-ray analysis of (a) PPy@TiB_2 and (b) Congo red-adsorbed PPy@TiB_2.

been considering polymeric nanoadsorbents based on polypyrrole for several years.

The polymer has many properties that make it an ideal solution for water pollution problems [12]. Scientists have found that polypyrrole-based nanocomposites effectively clean the environment of heavy metal ions and radioactive pollutants, pigments, chemical compounds, and pesticides. Recent studies highlight photovoltaic efficiency, optical features, degradation capacity of photocatalytic materials, physical characteristics, and electric characteristics [13–15]. The

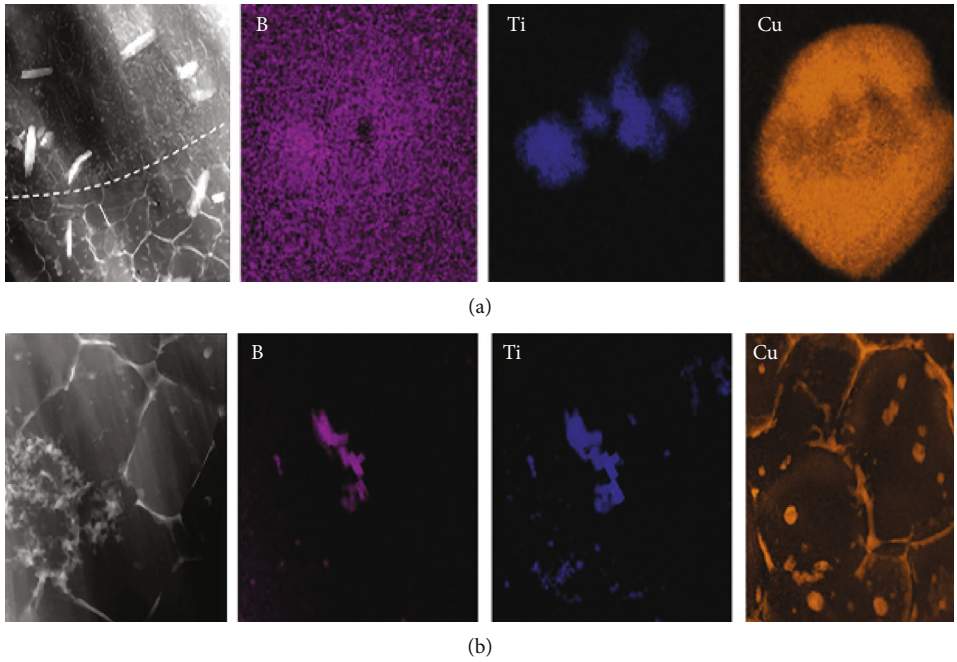

Figure 6: (a) PPy@TiB_2 and (b) process after Congo red-adsorbed PPy@TiB_2 elemental mapping analysis.

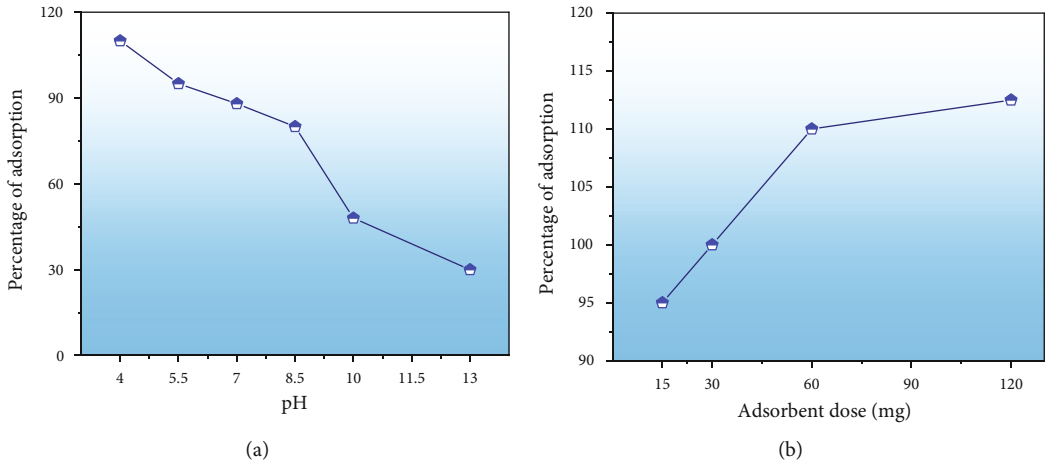

Figure 7: (a) Impact of pH and (b) impact of adsorbent dosage.

chemical polymerization production of polypyrrole-coated titanium diboride (PPy@TiB_2) has positively affected the environment. In the adsorption investigation, several traits and parameters were analyzed. Scientists have used the produced PPy@TiB_2 nanomaterial for wastewater dye removal due to its excellent performance and ease of reusing [16].

2. Experimentation

2.1. Methods and Materials. In the presence of a PPy monomer, a chemical polymerization approach is used to create a PPy@TiB_2 nanoadsorbent. There were 2 mL of pyrrole monomer and 30 minutes of ultrasonication at 27°C to prepare TiB_2 nanoparticles. The pyrrole monomer was allowed to adsorb on the TiB_2 nanoparticles' surfaces by swirling the dispersion for 60 minutes at 27°C [17, 18]. Iron was added to the TiB_2 dispersion as an oxidizing agent to polymerize the pyrrole on the nanoparticles' surfaces. The mixture was stirred for an additional 24 hours at 27°C using an electric stirrer. A four-hour oven drying at 100°C removed the contaminants and unreacted oxidants after cleaning the PPy@TiB_2 nanoadsorbent with deionized water and acetone after polymerization. An illustration of TiB_2 nanoparticles coated with polypyrrole is indicated in Figure 1.

2.2. Characterization. PPy@TiB_2 nanoadsorbent including TEM, HR-TEM, and fast Fourier transform (FFT) were synthesized. TESCAN FE-SEM, elemental mapping, and EDX analyze the PPy@TiB_2 nanoadsorbent earlier and the subsequent adsorption. X-ray diffraction measurements were determined using Cu Kα radiation with a 10° to 90° (2Θ) wavelength range [19]. The nitrogen adsorption technique

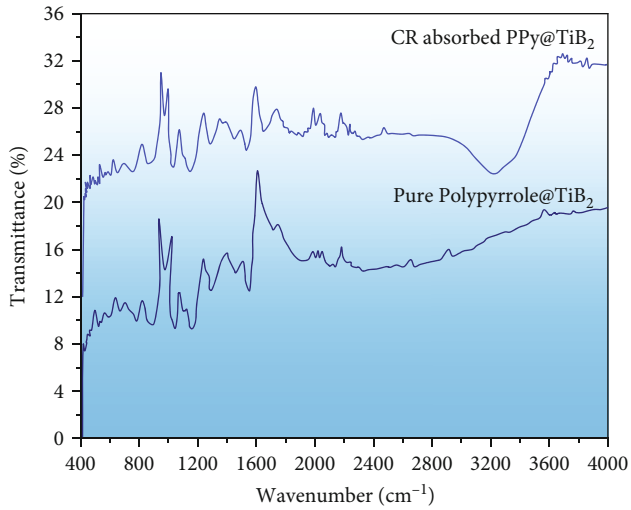

FIGURE 8: Image of attenuated total reflection-Fourier transform infrared spectroscopy.

measures pore size distributions and particular surface area. Using an FTIR spectrometer, it was necessary to conduct pre- and postadsorption studies on the nanoadsorbent, nano-PPy@TiB_2 [20].

2.3. Adsorption Studies. When removing Congo red (CR), batch experiments were carried out to test how the as-synthesized PPy@TiB_2 nanoadsorbent performed. The nanoadsorbent PPy@TiB_2 nanoadsorbent was studied to assess the effects of pH (acidity), contact time, and dosage on adsorption performance [21]. A pH experiment was conducted to check the PPy@TiB_2 nanoadsorbent-adsorbed CR at various pH levels (4 to 13). Adsorbent doses of 60 mg and 10 ppm of CR were used to test the adsorption performance. The synthetic nanoadsorbent was evaluated at various doses (15, 30, 60, and 120 mg) in a 10 ppm CR dye concentration to determine the effect of the dose [22]. Color concentrations were measured using a UV-V spectrophotometer during the batch adsorption trials. The formula used to calculate the percentage of CR dye that is eradicated is as follows [23, 24]:

$$\text{Percentage of Removal} = \frac{C_i - C_f}{C_i} \times 100 \quad (1)$$

C_i starting concentration of Congo red color
C_f CR dye's ending concentration

3. Results and Discussions

3.1. Properties of PPy@TiB_2 Nanoparticles. Investigation of PPy@TiB_2 nanocrystalline adsorbent structure was done using XRD. As-synthesized PPy@TiB_2 is indicated in Figure 2(a). Results showed that TiB_2 nanoparticles in composite form with PPy polymer were anatase crystalline. There were no visible phases other than TiB_2 in Figure 2(a), which verify the XRD pattern of its different stages (rutile and brookite). It discovered that PPy@TiB_2 nanocomposite reduced the crystalline phase of TiB_2 and PPy's amorphous nature by interacting with TiB_2. XRD data suggest that the surface morphology of TiB_2 nanoparticles with conducting polymer PPy was successful, as demonstrated by these results [25, 26]. Furthermore, TEM and HR-TEM analysis strongly support these findings.

Yet, Figure 2(b) shows the TEM patterns of the synthesized PPy@TiB_2. The TEM image of the synthesized PPy@-TiB_2 showed that only the TiB_2 facet had PPy polymer deposited on it, regardless of the other aspect [27]. A patch of unilluminated PPy polymer showed TiB_2 nanoparticles scattered everywhere, while PPy polymer granules with TiB_2 nanoparticles interacted tightly. TiB_2's high contrast made it distinct from PPy, which has lower contrast (Figure 2(b)). This nanoadsorbent formed using TiB_2 in the TEM image inset clearly showed the crystalline structure of the TiB_2 [28]. High resolution-TEM and FFT confirm that TiB_2 nanocomposite PPy@TiB_2 nanocomposite had an anatase crystalline phase as shown in supplemental Figures 3(a) and 3(b).

The surface, structural characteristics, and pore geometries of the PPy@TiB_2 nanospecific adsorbent were determined by the isotherm of nitrogen attachment shown in Figure 3(a). It reveals that saturation is observed at higher pressures, with a gradual increase in adsorption up to roughly 0.70 relative pressure (P/Po) [29]. Because of this, mesoporous adsorbents have a unique isotherm. The average pore diameters of the nanoadsorbent with 62.27 m_2/g surface area are 245.307 Å for adsorption and 216.698 Å for desorption using the nitrogen adsorption-desorption isotherm and the BJH technique [30]. In Figure 3(b), the average BET pore sizes for adsorption and desorption were 232.0041 Å and 247.2938 Å, respectively. According to IUPAC guidelines, mesoporous materials have pore diameters between 20 and 500 nm. Thus, the PPy@TiB_2 nanoadsorbent favours the mesoporous character of the material because of its pore sizes. Desorption is showed to be possible in Figure 3(a), where the desorption sum pore volume (0.385022 cm^3/gram) is greater than the adsorption sum pore volume (0.361217 cm^3/gram) at P/Po = 0.982. It shows that reversible desorption is conceivable. The regeneration results confirmed this tendency even more conclusively. A mesopore capillary condensation is present in the isotherm, in accordance with IUPAC's classifications of physisorption isotherm/hysteresis loops [31].

These images were taken at three different magnification levels and show the material's granular structure. As the magnification increased, the brightness decreased, indicating that the brightest particles were on the surface while the dullest particles were discovered deep within the layer (Figures 4(a) and 4(b)). It appeared like the character was uniform and smooth. Nanoparticles prepared before CR adsorption became more dispersed and bulkier in their microstructures.

Additionally, the components in the adsorbed PPy@TiB_2 were found out by FESEM-EDX analysis. As depicted in Figure 5, pure and CR-adsorbed PPy@TiB_2 samples have different elemental compositions. In the EDX spectra, carbon, oxygen, nitrogen, and titanium (Ti) are all visible (Figure 5(a)). Because of their relative atomic weights of

Table 1: Assignment of FTIR peaks in the pure and Congo red-adsorbed PPy@TiB_2.

FTIR peaks of PPy@TiB_2 (wavenumber cm^{-1})	Peaks role	FTIR peaks of Congo red-adsorped PPy@TiB_2 (wavenumber cm^{-1})	Peaks role
1537.64	Carbon-carbon pyrrole bond stretching vibration	1521.56	Carbon-carbon pyrrole bond stretching vibration
1447.79	Conjugated C-N band for stretching	1436.68	Conjugated C-N band for stretching
1291.17	A band of conjugated deformation in the plane of C-H	1272.28	A band of conjugated deformation in the plane of C-H
1142.18	Conjugated carbon-nitrogen stretching vibrations	1136.32	Conjugated carbon-nitrogen stretching vibrations
1034.13	Nitrogen-hydrogen in the planar deformation band	1025.04	Nitrogen-hydrogen in the planar deformation band
992.25, 882.29, 780.08	Deformations of the pyrrole ring G-H in and out of the plane	988.32, 860.58, 754.42	Deformations of the pyrrole ring G-H in and out of the plane
664.89	Characteristic peak of TiB_2	649.33	Characteristic peak of TiB_2
478.71	Stretching mode for the titanium-boride bond	477.51	Stretching mode for the titanium-boride bond

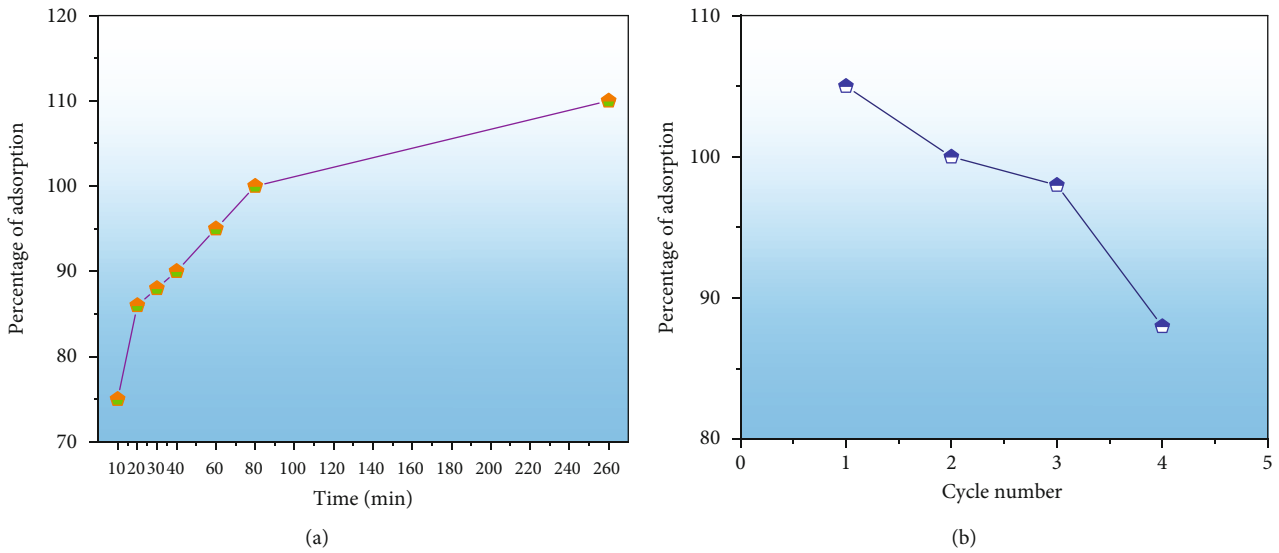

Figure 9: (a) Impact of contact duration and (b) regeneration capabilities of PPy@TiB_2 for Congo red dye adsorption.

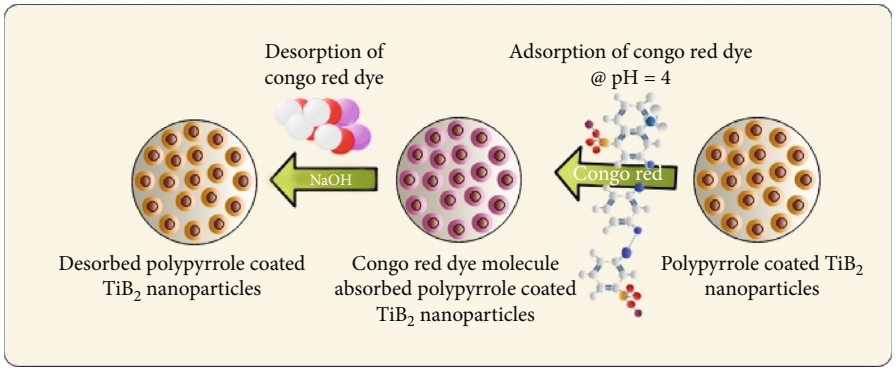

Figure 10: Diagram for adsorbed and desorbed mechanism of Congo red dye molecule on PPy@TiB_2.

50.75 and 28.21%, C and O atoms may have an effect on PPy@TiB_2's adsorption to CR dye molecules. In Figure 5(b), Na, C, and O atoms with high atomic masses indicate as evidence that CR molecules adsorb onto PPy@-TiB_2. Elements in PPy@TiB_2 and CR-adsorbed PPy@TiB_2 were studied further by an elemental mapping experiment [32, 33]. Before and after CR dye adsorption on PPy@TiB_2, the elemental mapping is indicated in Figure 6. In the PPy@-TiB_2 nanoadsorbent, carbon, oxygen, nitrogen, and titanium were all evenly distributed. C, O, and Na distributions were validated by exposing the nanoadsorbent PPy@TiB_2 nanoadsorbent to CR molecules [32, 33].

3.2. Behaviour of Adsorption

3.2.1. Impact of pH. When the aqueous phase's pH alters, it alters both the binding sites and ionization processes in this experiment [34, 35]. Figure 7(a) illustrates the percentage of Congo red adsorption by PPy@TiB_2 at different pH values (4.0, 5.5, 7, 8.5, 10.0, and 13.0). The starting pH level of 4.0 (98.75%) had the highest adsorption rate, which decreased as the pH increased. Positively charged PPy@TiB_2 surface was inhibited by electrostatic contact with negatively charged CR (due to the presence of two $-SO_3$ groups) [36]. Both Congo red and PPy@TiB_2 became negatively charged as the pH increased and the adsorption percentage reduced [37].

3.2.2. Effect of Adsorbent Dose. The amount of PPy@TiB_2 used had a beneficial impact on the adsorption percentage (Figure 7(b)). The percentage of adsorption rate was increased to obtain the equilibrium state of maximum adsorption [38]. Adsorption on the PPy@TiB_2 surface increases when the dose increases as the number of adsorption sites increases. The optimum PPy@TiB_2 amount attains to be 0.05 gm due to this study.

The AT-FTIR spectrum of pure PPy@TiB_2 and that of CR-adsorbed PPy@TiB_2 is indicated in Figure 8. Band assignments and wavenumbers are shown in Table 1 for the two samples, including the pure TiB_2 and TiB_2+CR-adsorbed PPy@TiB_2 FTIR bands. Most peaks experienced a minor shift to the lower wavenumbers after CR dye adsorbs on PPy@TiB_2 [39]. Therefore, these shifting peak values make it clear that the CR dye was successfully adsorbing onto PPy@TiB_2.

3.2.3. Effect of Adsorption Time. In adsorption experiments, adsorption time is critical. CR adsorption is illustrated in various time intervals in Figure 9(a). During the first 30 minutes of the investigation, the percentage of CR slowly adsorbing into the PPy@TiB_2 grew dramatically, reaching a maximum (110%) after 260 minutes. CR adsorption was stable, indicating that it attains the equilibrium phase. For the nanoadsorbent PPy@TiB_2 nanoadsorbent, 260 minutes show the optimal duration for carbon dioxide adsorption. When PPy@TiB_2 is adsorbed, the diffusion process is evidenced by the gradual rise in the adsorbed percentage [40].

3.2.4. Regeneration Study. The exhausted adsorbent (Congo red-adsorbed PPy@TiB_2) was evaluated on how well it can revitalize in a regeneration study [41]. It is shown in Figure 9(b) that NaOH was used as a desorbing agent for four cycles. This PPy@TiB_2 nevertheless showed outstanding regeneration efficacy with an adsorption decrease from 98.75 to 97% in Figure 9(b). PPy@TiB_2 proves to be a valuable and economical material for removing CR. The reproducibility of PPy@TiB_2 for eliminating CR from textile wastewater was established.

3.2.5. Adsorption Mechanism. The dynamic, active sites on the PPy@TiB_2 surface allowed CR to adsorb on it. A schematic diagram of CR dye molecule adsorption and desorption onto PPy@TiB_2 nanoadsorbent is indicated in Figure 10. Chemical polymerization was employed to synthesize nanocomposite using TiB_2 nanoparticles. Dispersed TiB_2 nanoparticles were used to adsorb the Polypyrrole monomer. Then, the pyrrole-adsorbed TiB_2 dispersal is treated with the $FeCl_3$ solution as an oxidizing agent. Finally, CR adsorption was determined using the polymerized PPy@TiB_2 nanoadsorbent. Carbo-oxygen-nitrogen-titanium elements make up its surface. Adsorption of textile wastewater is made more accessible with the final polymer form's increased surface area and chemical functionality. This positive charge is created by protonating the PPy@TiB_2 surface functional groups at pH = 4. This positive charge is used to interact with CR's negative $-SO_3$ groups. Due to the negative CR's electrostatic attraction to the TiB_2 surface, the adsorption is reduced as pH rises, whereas deprotonation caused a decrease in surface charge density.

4. Conclusion

Chemical polymerization with pyrrole (monomer) and ferric chloride successfully converted tiny titanium diboride nanoparticles (oxidizing agent). Polypyrrole originates on the surface of TiB_2 nanocomposites. PPy@TiB_2 nanoparticles were formed, and CR molecules could adhere to them, according to spectroscopic, structural, and morphological studies. It discovered that pH = 4260 minutes of contact hours, 60 mg of adsorbent, and a Congo red dye concentration of 10 ppm were the ideal adsorption conditions. After four cycles, a nanoadsorbent could maintain 90% of the CR color. The outcomes show that polypyrrole-coated titanium oxide nanoparticles are an effective treatment option for colored wastewater containing dye.

Data Availability

All authors confirmed that all necessary data are available in the manuscript.

Conflicts of Interest

The authors declare that they have no conflicts of interest.

References

[1] U. Sudhakara and J. Srinivasb, "Mechanical characteristics and corrosion behavior of friction stir AA5251-AA6063 butt

welds," *Materials Today: Proceedings*, vol. 15, pp. 132–137, 2019.

[2] Rajesh and P. Kaushik, "Micro structural behavior analysis of friction stir processed Al alloy AA6063/SIC," *The International Journal of Mechanical Engineering and Technology*, vol. 8, no. 11, pp. 991–998, 2017, [Online]. Available: https://www.scopus.com/inward/record.uri?eid=2-s2.0-85036561589&partnerID=40&md5=9100d82d683bd81f02d51a289c90ec1e.

[3] T. Teker, T. Kurşun, and T. Kurşun, "Weldability of AA6063 alloys by using keyhole gas tungsten arc welding technique," *Kovove Materialy-Metallic Materials*, vol. 52, no. 4, pp. 237–242, 2021.

[4] I. Sabry, A. M. El-Kassas, A.-H. I. Mourad, D. T. Thekkuden, and J. A. Qudeiri, "Friction stir welding of T-joints: experimental and statistical analysis," *Journal of Manufacturing and Materials Processing*, vol. 3, no. 2, 2019.

[5] R. Ramamoorthi, K. P. Yuvaraj, C. Gokul, S. J. Eashwar, N. Arunkumar, and S. A. T. Dheen, "An investigation of the impact of axial force on friction stir-welded AA5086/AA6063 on microstructure and mechanical properties butt joints," *Materials Today: Proceedings*, vol. 37, Part 2, pp. 3159–3163, 2021.

[6] Z. Ahmadi, M. Zakeri, M. Farvizi, A. Habibi-Yangjeh, S. Asadzadeh-Khaneghah, and M. Shahedi Asl, "Synergistic influence of SiC and C3N4 reinforcements on the characteristics of ZrB2-based composites," *Journal of Asian Ceramic Societies*, vol. 9, no. 1, pp. 53–62, 2021.

[7] N. Kaushik, S. Singhal, P. G. Rajesh, and B. N. Tripathi, "Experimental investigations of friction stir welded AA6063 aluminum matrix composite," *Journal of Mechanical Engineering Science*, vol. 12, no. 4, pp. 4127–4140, 2018.

[8] A. Sharma and D. B. Karunakar, "Effect of SiC and TiC addition on microstructural and mechanical characteristics of microwave sintered ZrB_2 based hybrid composites," *Ceramics International*, vol. 47, no. 18, pp. 26455–26464, 2021.

[9] S. A. A. Alem, R. Latifi, S. Angizi et al., "Development of metal matrix composites and nanocomposites via double-pressing double-sintering (DPDS) method," *Materials Today Communications*, vol. 25, p. 101245, 2020.

[10] S. A. Delbari, J. Lee, M. Sheikhlou et al., "Effect of iron nanoparticles on spark plasma sinterability of ZrB2-based ceramics," *Journal of the Australian Ceramic Society*, vol. 58, no. 4, pp. 1117–1128, 2022.

[11] E. S. Motailo, L. A. Lisyanskii, S. V. Vikhman, and D. D. Nesmelov, "Physical and mechanical properties of composite ceramics in the ZrB2–SiC–MoSi2 system," *Glass Physics and Chemistry*, vol. 47, no. 6, pp. 646–652, 2021.

[12] M. Shahedi Asl, Y. Azizian-Kalandaragh, Z. Ahmadi, A. Sabahi Namini, and A. Motallebzadeh, "Spark plasma sintering of ZrB2-based composites co-reinforced with SiC whiskers and pulverized carbon fibers," *International Journal of Refractory Metals and Hard Materials*, vol. 83, article 104989, 2019.

[13] T. Chen, W. Lu, Y. Fu, T. Chen, and W. Li, "Synthesis and characterization of chrom-free Zr-Ti-Ni pale green coating on AA6063 aluminium alloy," *Advanced Materials Research*, vol. 1053, pp. 414–420, 2014.

[14] V. A. Shcherbakov, A. N. Gryadunov, Y. N. Barinov, and O. I. Botvina, "Synthesis and properties of composites based on zirconium and chromium borides," *Russian Journal of Non-Ferrous Metals*, vol. 60, no. 2, pp. 179–185, 2019.

[15] B. Mohammadzadeh, S. Jung, T. H. Lee et al., "Characterization and FEA evaluation of a ZrB_2-SiC ceramic containing TaC for beam-column joint application," *Ceramics International*, vol. 47, no. 8, pp. 11438–11450, 2021.

[16] A. D. Sytchenko, S. B. Kabildina, and P. V. Kiryukhantsev-Korneev, "Effect of nitrogen concentration in a gas mixture on the structure and properties of Zr–B–(N) coatings obtained by the HIPIMS methods," *Russian Journal of Non-Ferrous Metals*, vol. 62, no. 6, pp. 785–793, 2021.

[17] S. Cheneke and D. Benny Karunakar, "The effect of solution treatment on aging behavior and mechanical properties of AA2024-TiB2 composite synthesized by semi-solid casting," *SN Applied Sciences*, vol. 1, no. 11, pp. 1–17, 2019.

[18] S. C. Lemessa and D. B. Karunakar, "Characterization and mechanical properties of 2024/Y2O3 composite developed by stir rheocasting," *Lecture Notes in Mechanical Engineering.*, vol. 1, pp. 439–453, 2020.

[19] S. Cheneke and D. B. Karunakar, "Microstructure characterization and evaluation of mechanical properties of stir rheocast AA2024/TiB2 composite," *Journal of Composite Materials*, vol. 54, no. 7, pp. 981–997, 2020.

[20] Y. R. Wang, C. J. Jin, and J. I. Song, "Mechanical characteristics of Al2O3, TiO2 and Al2O3-40.wt%TiO2 thermal coating on AISI 1045 matrix by nano-indentation test," *8th Asian-Australasian Conference on Composite Materials 2012, ACCM 2012 - Composites: Enabling Tomorrow's Industry Today,*, vol. 1, pp. , 2012639–645, 2012, [Online]. Available: https://www.scopus.com/inward/record.uri?eid=2-s2.0-84892991822&partnerID=40&md5=acf24a5e41c4f2209d799b3f515de0cd.

[21] C. Badini, P. Fino, M. Musso, and P. Dinardo, "Thermal fatigue behaviour of a 2014/Al_2O_3-SiO_2 (Saffil® fibers) composite processed by squeeze casting," *Materials Chemistry and Physics*, vol. 64, no. 3, pp. 247–255, 2000.

[22] O.-G. Lademo, O. S. Hopperstad, and M. Langseth, "An evaluation of yield criteria and flow rules for aluminium alloys," *International Journal of Plasticity*, vol. 15, no. 2, pp. 191–208, 1999.

[23] J. Feng, X. Du, Y. Sun, K. Zhao, Z. Shi, and M. Liu, "Effect of La–O–S complex inoculant on microstructure and mechanical characteristics of ductile iron," *Journal of Materials Science*, vol. 57, no. 8, pp. 5288–5297, 2022.

[24] S. Dharani Kumar and S. Sendhil Kumar, "Investigation of mechanical behavior of friction stir welded joints of AA6063 with AA5083 aluminum alloys," *Mechanics and Mechanical Engineering*, vol. 23, no. 1, pp. 59–63, 2019.

[25] T. S. Mahmoud, "Effect of friction stir processing on electrical conductivity and corrosion resistance of AA6063-T6 Al alloy," *Proceedings of the Institution of Mechanical Engineers, Part C: Journal of Mechanical Engineering Science*, vol. 222, no. 7, pp. 1117–1123, 2008.

[26] M. Abu-Okail, N. A. Alsaleh, W. M. Farouk et al., "Effect of dispersion of alumina nanoparticles and graphene nanoplatelets on microstructural and mechanical characteristics of hybrid carbon/glass fibers reinforced polymer composite," *Journal of Materials Research and Technology*, vol. 14, pp. 2624–2637, 2021.

[27] T. Kannan, B. Arulmurugan, L. Feroz Ali, and L. Rajeshkumar, "Performance analysis of AA3103 and AA6063 dissimilar weld joints by friction stir welding," *Songklanakarin Journal of Science & Technology*, vol. 44, no. 2, pp. 316–322, 2022, https://www.scopus.com/inward/record.uri?eid=2-s2.0-

8 5 1 3 2 8 9 7 8 7 2 & p a r t n e r I D = 4 0 & m d 5 = 28f9d950f7503bca3caec366bfa43639.

[28] T.-Y. Chen, W. Lu, W.-F. Li, and Y.-Q. Fu, "Synthesis of chrome-free coloring conversion coating on AA6063 aluminium alloy and its electrochemical properties," *Cailiao Gongcheng/Journal Materials Engineering*, vol. 43, no. 12, pp. 52–57, 2015.

[29] F. O. Edoziuno, A. A. Adediran, B. U. Odoni, O. G. Utu, and A. Olayanju, "Physico-chemical and morphological evaluation of palm kernel shell particulate reinforced aluminium matrix composites," *Materials Today: Proceedings*, vol. 38, pp. 652–657, 2021.

[30] O. S. I. Fayomi, O. P. Gbenebor, M. Abdulwahab, C. A. Bolu, and A. P. I. Popoola, "Structural modification, strengthening mechanism and electrochemical assessment of the enhanced conditioned AA6063-type Al-mg-Si alloy," *Journal of New Materials for Electrochemical Systems*, vol. 16, no. 1, pp. 59–64, 2013.

[31] D. Özyürek, T. Tunçay, and H. Kaya, "The effects of t5 and t6 heat treatments on wear behaviour of aa6063 alloy," *High Temperature Materials and Processes*, vol. 33, no. 3, pp. 231–237, 2014.

[32] G. N. Kumar, V. M. Reddy, Y. V. M. Reddy, and K. H. Reddy, "Study of abrasive wear behavior of AA 6063/TICP In-situ composites," *International Journal of Mechanical Engineering and Technology*, vol. 8, no. 5, pp. 42–52, 2017, [Online]. Available: https://www.scopus.com/inward/record.uri?eid=2-s2.0-8 5 0 1 9 5 5 0 6 2 6 & p a r t n e r I D = 4 0 & m d 5 = 0627f78d6d5367e54b06132b8dfa5740.

[33] P. Sureshkumar and V. C. Uvaraja, "Effect of ceramic and metallic reinforcement on mechanical, corrosion, and tribological behavior of aluminum composite by adopting design of experiment through Taguchi technique," *Journal of Tribology*, vol. 140, no. 5, 2018.

[34] N. Kaushik and S. Singhal, "Experimental investigations on microstructural and mechanical behavior of friction stir welded aluminum matrix composite," *International Journal of Engineering*, vol. 32, no. 1, pp. 162–170, 2019.

[35] O. S. I. Fayomi, I. G. Akande, A. P. I. Popoola, and H. Molifi, "Potentiodynamic polarization studies of cefadroxil and dicloxacillin drugs on the corrosion susceptibility of aluminium AA6063 in 0.5 M nitric acid," *Journal of Materials Research and Technology*, vol. 8, no. 3, pp. 3088–3096, 2019.

[36] T. Chen, W. Lu, W. Li, and Y. Fu, "Preparation and performace of a black-grey coating on AA6063 aluminium alloy," *Journal of Chinese Society for Corrosion and protection*, vol. 35, no. 2, pp. 177–182, 2015.

[37] T. Chen, Y. Fu, W. Lu, T. Chen, and W. Li, "Synthesis and characterization of chrom-free dark coating on AA6063 aluminium alloy with K2ZrF6," *Advanced Materials Research*, vol. 1053, pp. 421–428, 2014.

[38] S. Arnuri and S. N. Gurugubelli, "The effect of T8 heat treatment on wear behaviour and microstructure of 6063 aluminium alloy deformed by Cryo and RT ECAP," *Minerals, Metals and Materials Series*, pp. 1727–1741, 2021.

[39] A. Sabahi Namini, S. A. Delbari, M. Shahedi Asl, Q. V. Le, and M. Shokouhimehr, "Characterization of reactive spark plasma sintered (Zr,Ti)B2-ZrC-SiC composites," *Journal of the Taiwan Institute of Chemical Engineers*, vol. 119, pp. 187–195, 2021.

[40] E. R. Ferkhatly, A. V. Kovalska, and Y. I. Bogomol, "Microstructure and micromechanical properties of directionally crystallized composites of the B4C–(TixZr1 – x)B2 system," *Journal of Superhard Materials*, vol. 44, no. 2, pp. 111–116, 2022.

[41] V. A. Shcherbakov, A. N. Gryadunov, and M. I. Alymov, "Microstructural features of SHS-pressing ZrB2-B4C and TiB2-B4C composites," *Letters on Materials*, vol. 9, no. 1, pp. 11–16, 2019.